

Transformation of Microstructure and Mechanical Properties in the Machined Surface of Powder Metallurgy Superalloy

Du Jin, Zhang Jingjie, Wang Ligu

Qilu University of Technology, Jinan 250353, China

Abstract: During the machining of powder metallurgy (PM) superalloy parts, the machined surface bears severe plastic deformation which leads to the transformation of microstructure and mechanical properties. White layer which reflects the transformation of microstructure and mechanical properties, often appears on the top of machined surface during hard machining of PM superalloy. White layer has significant effect on the machined surface integrity. The effects of cutting speed on the white layer formation have been investigated in order to reveal the transformation of the microstructure and mechanical properties in the machined surface of PM superalloy FGH95. Results show that white layer thickness increases with the increasing of cutting speed. The machined surface exhibits densification with no obvious structural characteristics. FGH95 superalloy bulk material exists in the form of Ni-based solid solution, while the microstructure of white layer is significantly different from that of bulk materials. It's because of the microstructure of Ni-based solid solution which has transformed during the cutting of FGH95. The higher the cutting speed is, the more obvious the grain refinement is. A higher cutting speed could also lead to higher values of hardness in white layer. Residual stresses in the machined surface of FGH95 are tensile in all cutting conditions, which show an increasing trend with the increasing of cutting speed. This research can provide the theoretical basis for the investigation and controlling of machined surface quality.

Key words: powder metallurgy; machined surface; phase transformation; hardness measurement; residual stress

Ni-based superalloy FGH95 produced through powder metallurgy (PM) process has been recently developed for aero engine turbine and disc applications, which require high strength and creep resistance at elevated temperature (700~900 °C). Although FGH95 superalloy is formed by powder metallurgy process which can produce near net shape parts, finishing operations such as cutting, and burnishing are still essential to meet the tolerance requirements or to achieve better surface quality. However, Ni-based superalloy is extremely difficult to machine due to its several inherent properties, including low thermal conductivity that leads to elevated temperature at the tool/chip interface during machining, work hardening tendency during machining that becomes more severe with increased strengthening of this superalloy, and intensive adhesion to the surface of the tooling during machining processes^[1-5]. The transformation of

microstructure and mechanical properties occurs in the machined surface due to the severe plastic deformation during the machining of FGH95. More seriously, white layer appears on the top of machined surface owing to its high loads and high temperatures during the hard machining. White layer is one of the outcomes of microstructure and mechanical properties transformation in the machined surface. It becomes white after etching when observed under a light optical microscope or featureless in scanning electron microscopy (SEM)^[6]. White layer is generally described as consisting of a refined structure with a grain size of several tens of nanometers. Herbert and Axinte^[7] reported that the white layer generated from non-standard drilling parameters in alloy RR1000 was face centre cubic (fcc) in structure and polycrystalline with an average grain size of 50nm compared to the bulk material of 22~63 μm (ASTM 8-5). Bushlya^[8]

Received date: August 25, 2017

Foundation item: National Natural Science Foundation of China (51405254); Special Grade of the Financial Support from the China Postdoctoral Science Foundation (2015T80712); Shandong Province Postdoctoral Innovation Project Special Funds (2014M561919)

Corresponding author: Du Jin, Ph. D., Associate Professor, School of Mechanical & Automotive Engineering, Qilu University of Technology, Jinan 250353, P. R. China, E-mail: dj84105@126.com

Copyright © 2018, Northwest Institute for Nonferrous Metal Research. Published by Elsevier BV. All rights reserved.

used high resolution transmission electron microscopy (HRTEM) to observe the white layer on the machined surface of aged Inconel 718 and revealed the formation mechanism of nanostructured material with grain size of 50~150 nm. Phase composition of white layer was found to include phases of the parent bulk material. It was believed that the refinement of grain size was predominantly attributed to dynamic recrystallization and grain subdivision by severe plastic deformation of the near surface region. The characteristics of white layer were commonly recognized as resistance to etch by conventional methods, high microhardness and increased wear resistance^[9-12]. Herbert^[7] also presented that the white layer had a hardness 45% higher than the bulk material. Ranganath^[13] reported that the hardness of white layers was 2~3 times higher than that of the bulk material in low cutting speed cases with blunt edged tools (large edge radius, negative effective rake angle) in the machining of Ni-based superalloy. Aramcharoen^[14] investigated that the white layer formed at 200 m/min has extremely high hardnesses which are 41%, 36% and 33% more than that of bulk materials for uncoated carbide, CrTiAlN and CrTiAlN+MoST coated tools, respectively. Guo and Schwach^[15] reported that the white layer was 30%~60% harder than bulk material. Furthermore, the hardness of white layers had a general increase trend with the increase of cutting speed. Akcan and Shan reported that white layer had a hardness of 12.85 ± 0.80 GPa, which was about 25% higher than that of the hardest martensitic structures^[16]. The thickness of white layer increased with elevation in cutting parameters^[17]. With increase in feed rate and cutting speed, cutting temperature increased. At the same time, strain rate in cutting region also increased resulting in a higher amount of plastic deformation and hence induced the rising of white layer thickness. However, variation of white layer with cutting speed was not always consistent^[18,19]. Decrease in white layer thickness with increase in cutting speed was also observed^[15,20]. One of the possible explanations might be lower residence time of moving heat source, reducing the level of thermal energy transferred to machined surface although temperature of cutting edge was higher. Therefore, regarding the white layer formation mechanisms and the resulting microstructural constituents the results vary a lot. Depending on the machining parameters, possible white layer formation mechanisms had been suggested to be either mainly thermally induced through phase transformations or mainly mechanically induced through severe plastic deformation^[21]. Some researchers had investigated the influences of cutting speed and tool flank wear on white layer. Hosseini^[22,23] reported that white layer could be formed either below ~540 °C or above ~920 °C Ac1. The authors concluded that the formation mechanism of the mechanically induced white layer was dominated by dynamic recovery where the microstructure was characterized by a broken-down and elongated sub-structure containing severely elongated secondary carbides. In

thermally induced white layer, the microstructural evolution was initiated by dynamic recovery, which advanced to dynamic recrystallization at the increased temperatures caused by the higher cutting speeds. The microstructure of the thermally induced white layer was characterized by equiaxed grains that resemble recrystallized grains and by the elongated and broken-down sub-surface.

Yet, the formation of white layer poses a significant potential danger to fatigue life of machined surface^[24,25]. Guo and Warren^[26] reported that a turned white layer surface by a worn tool generates a high tensile stress in the area of the white layer, but becomes more highly compressive in the deeper subsurface than the turned one without a white layer. They further concluded that no white layer samples were more resistive to fatigue crack initiation/propagation and, therefore had a longer life when compared to the white layer samples with equivalent surface finish^[27]. White layer also reduced the damping capacity of machined parts. Siva^[28] proposed that the machined specimen exhibited low damping values which can be attributed to the formation of white layer acting as a protective layer to dissipate elastic strain energy which results in reduction of damping values.

The fatigue life of a machined part depends strongly on its surface quality^[29]. Since the FGH95 superalloy is used in critical engine components, the fatigue life and damping capacity must be resolved first. Therefore, the formation of white layer on the parts machined surface must be considered after the machining. At present, few studies are carried out on the white layer formation mechanism and its mechanical properties in the machining of PM superalloy. There is also a lack of researches on the influences of cutting speed on the white layer formation in the machining of FGH95. Therefore, the aims of this study are to investigate the transformation of microstructure and mechanical properties in the machined surface and then illustrate the mechanism of white layer formation in the machining of PM superalloy FGH95. The cutting experiments with various cutting speeds were carried out to study the effects of cutting speeds on the white layer formation. SEM with Energy Dispersive Spectrometer (EDS) and X-ray Diffraction (XRD) were employed to analyze the bulk material and white layer's chemical elements and microstructure so as to reveal the mechanism of white layer formation. The measurements of microhardness and residual stress on the machined surface were taken to test the mechanical properties of white layer. This study can provide theoretical guidance on the investigation of machined surface integrity in hard machining of Ni-based superalloy. It also has an important role in the optimization of cutting parameters so that improves the surface integrity of Ni-based superalloy.

1 Experiment

1.1 Workpiece material and cutting tool

The material applied in the cutting tests was FGH95

Ni-based PM superalloy. The chemical composition of FGH95 is shown in Table 1^[30].

The FGH95 superalloy was cut-off into sheet specimens in order to mount it in a special fixture as shown in Fig.1. The cutting tool employed in this experiment was face milling cutter supplied by KENNAMETAL INC. The cutting inserts were SNHX12L5PZTNGP KC725M with TiN, AlTiN advanced PVD coatings. Before each test cutting, the insert was changed to a fresh one in order to eliminate the influence of tool wear on the machined surface integrity.

1.2 Orthogonal milling tests

Cutting tests were carried out on a 3-axis CNC machining center with a maximum spindle rotation speed 10 000 r/min. The experimental setup is shown in Fig.1. In this study, the thickness, grain refinements, and microhardness of white layer and residual stress in machined surface were investigated with the cutting speeds. The cutting speeds employed in this experiment were 40, 80, 120, 160 and 200 m/min. The constant axial depth of cut and radial depth of cut were maintained at 2 and 0.5 mm, respectively. The feed was 0.02 mm/r.

After each cutting path, the machined workpiece sheet was cut-off into the square specimens (10 mm×10 mm) in order to mount in the Bakelite. Then, the samples were polished and etched with 2.5% copper chloride, 48.8% hydrochloric acid, and 48.7% ethanol to analyze possible metallurgical changes beneath the machined surfaces using optical microscope and SEM. EDS and XRD were employed to analyze the chemical elements and microstructure of machined surface and bulk materials. Vickers microhardness tester was applied to measure the microhardness of the machined surface white layer and bulk material. X-ray stress tester was used to measure the residual stress in the machined surface perpendicular to the direction of feed.

2 Results and Discussion

2.1 Microstructure of white layer

Table 1 Chemical composition of FGH95 (wt%)^[30]

C	Co	Cr	W	Mo	Al	Nb	Ni
0.06	8.00	12.98	3.40	3.40	3.48	3.50	Bal.

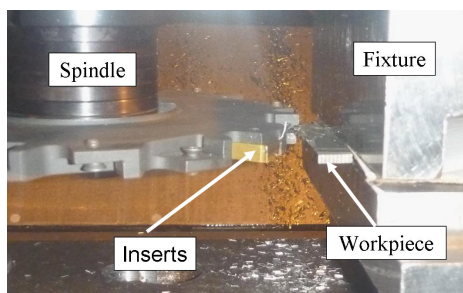


Fig.1 Workpiece and cutting inserts employed in the cutting tests

2.1.1 Metallographic of white layer

The metallographic samples of machined FGH95 were etched using copper sulfate solution, and then observed under optical microscope and SEM. The optical and SEM images of white layer on machined FGH95 surface are shown in Fig.2. It can be seen from Fig.2a that microstructures and grain boundaries in FGH95 superalloy bulk are visible clearly, which show different structure characteristics on the machined surface or subsurface. The machined surface of FGH95 superalloy covers a thin layer, which is bright white under the optical microscope, that is white layer. The microstructure of white layer under the SEM is shown in Fig.2b. This layer exhibits significantly different microstructures from that of bulk materials. It shows densification, with no obvious structural features. From Fig.2a, a dark region appears beneath the white layer, which is called transition zone or plastic flow layer^[31]. This region shows a strong plastic deformation flows along the cutting direction. It proves that the material plastic flow occurs along the cutting direction in the cutting process. From Fig. 2, the machined subsurface of FGH95 can be divided into two zones. One is white layer; the other is transition zone or plastic flow layer.

The thickness of white layer generated at different cutting speeds is exhibited in Fig.3. It can be seen from Fig.3 that cutting speeds have significant effects on the white layer thickness. The increasing of cutting speed increases the white layer thickness when other cutting parameters remain unchanged. This conclusion is the same as Attanasio's measurement results^[10], because of a large amount of heat energy generated from plastic deformation during high speed

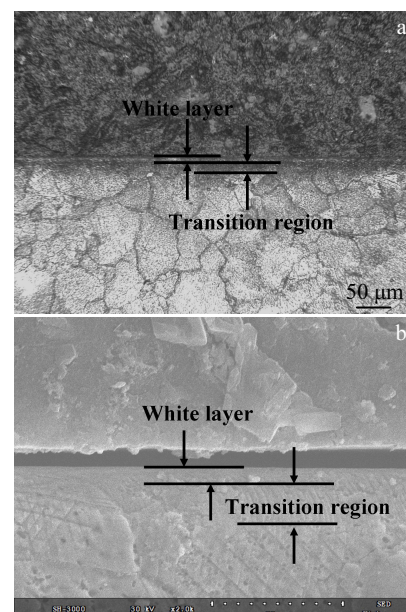


Fig.2 Microstructures of FGH95 machined surface: (a) optical image and (b) SEM image

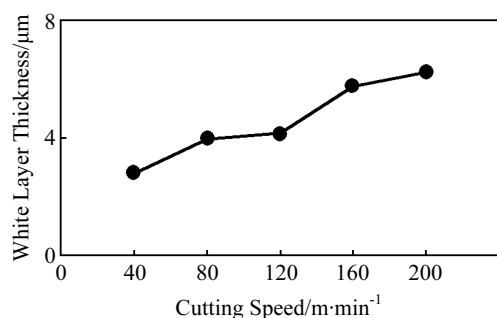


Fig. 3 Variation of white layer thickness with cutting speed

machining process. In addition, higher cutting speed means higher compressive forces acting on the machined surface, which can induce severe plastic deformation on the machined surface. With the increasing of cutting speed, the coupling of high temperature and severe plastic deformation can lead to the increasing of white layer thickness.

2.1.2 EDS analysis of white layer

EDS analysis was applied to obtain the element composition. It can be used for semi-quantitative element point analysis, line analysis and surface analysis. The element line analysis can be used to determine the element distribution along the specified direction. The EDS line analysis for machined surface of FGH95 along the direction of depth of cut is exhibited in Fig.4, the line with different color means different element distribution along the direction of depth of cut.

EDS analysis of white layer on the machined surface and bulk materials is listed in Fig.5. It can be clearly seen that the element contents of Ti and Nb in white layer are higher and the element contents of Cr and Co are lower than that of the bulk material. It can be inferred that the strengthening phase γ' content increases by 8%~15% according to the content of elements Ti, Nb in strengthening phase γ' while the elements Cr, Co are mainly in bulk phase γ , which shows that strengthening phase γ' precipitate dispersion appears during the machining. In addition, the element C and O contents increase more obviously in white layer. It can be drawn that the oxide and carbide contents increase in white layer because the workpiece material undergoes chemical reaction with the

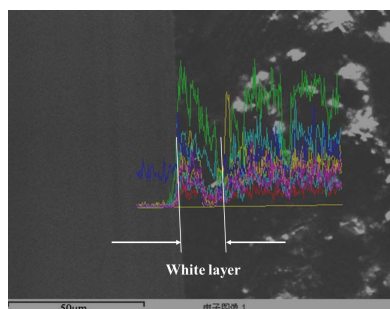


Fig. 4 EDS line scanning for FGH95 machined surface

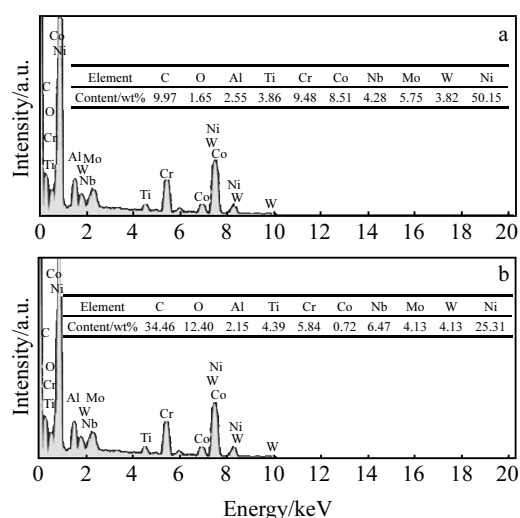


Fig. 5 EDS analysis for bulk materials (a) and white layer (b)

air at the elevated temperature and high pressure during machining process.

2.1.3 Phase analysis of white layer

X-ray diffraction (XRD) technique is commonly used for the analysis of material phase, grain size, lattice distortion measurement and the determination of crystallinity. In this section, XRD was employed for the analysis of white layer and bulk material phase transformation. The analyses are shown in Fig.6. The results show that the FGH95 alloy exists in the form of Ni-based solid solution. The solutes of Ni-based solid solution in FGH95 bulk materials are Al, Cr, W, Ta, Nb, Mo, Co, etc. The retrieved phases have a high matching with XRD PDF cards. XRD phase analyses also show that the white layer exists in the form of Ni-based solid solution, and the solute elements are Al, Cr, W, Ta, Nb, Mo, Co, etc. However, the white layer retrieved phase FOM value is higher than that of the bulk materials. It indicates that the retrieved phases in white layer have a low matching with XRD PDF

40 Hits Sorted on Figure-Of-Merit			FOM	a
	Chemical Formula			
<input type="checkbox"/> Aluminum Chromium Cobalt T...	Al _{0.34} Co _{0.41} Cr _{0.2...}		3.0	
<input type="checkbox"/> Nickel Tantalum	Ni _{0.9} Ta _{0.1}		3.3	
<input type="checkbox"/> Nickel Niobium	Nb _{0.1} Ni _{0.9}		3.3	
<input type="checkbox"/> Aluminum Nickel Tantalum	Al _{2.6} Ni _{10.7} Ta		3.4	
<input type="checkbox"/> Nickel Tungsten	Ni ₁₇ W ₃		3.5	
<input type="checkbox"/> Chromium Cobalt Molybdenu...	Ni-Cr-Co-Mo		5.6	
<input type="checkbox"/> Cobalt Carbide	CoC _x		11.7	
<input type="checkbox"/> Molybdenum Nickel	MoNi ₄		43.3	
<input type="checkbox"/> Cobalt Titanium	TiCo ₃		46.0	
40 Hits Sorted on Figure-Of-Merit			FOM	b
	Chemical Formula			
<input type="checkbox"/> Nickel Tungsten	Ni ₁₇ W ₃		16.3	
<input type="checkbox"/> Nickel Tantalum	Ni _{0.9} Ta _{0.1}		19.8	
<input type="checkbox"/> Nickel Niobium	Nb _{0.1} Ni _{0.9}		19.8	
<input type="checkbox"/> Molybdenum Nickel	MoNi ₄		23.2	
<input type="checkbox"/> Aluminum Chromium Cobalt T...	Al _{0.34} Co _{0.41} Cr _{0.2...}		34.6	
<input type="checkbox"/> Cobalt Titanium	TiCo ₃		39.2	
<input type="checkbox"/> Aluminum Nickel Tantalum	Al _{2.6} Ni _{10.7} Ta		43.6	
<input type="checkbox"/> Chromium Cobalt Molybdenu...	Ni-Cr-Co-Mo		45.3	
<input type="checkbox"/> Aluminum Nickel Niobium	AlNbNi ₂		48.2	

Fig. 6 XRD phase analysis for bulk materials (a) and white layer (b)

cards. It can be drawn that Ni-based solid solution of FGH95 alloy generates phase transformation during cutting process. Some experts believe that plastic deformation in the machining process plays an essential role in phase transformation below the nominal phase transformation temperature^[32].

2.2 Grain refinement in white layer

Metallographic images of FGH95 bulk materials and machined surface obtained at various cutting speeds were recorded by metallurgy observations. IPP software was employed to deal with the metallographic pictures, and outline the grain boundaries in the area of $227\ \mu\text{m} \times 174\ \mu\text{m}$. The equivalent diameter of grain was measured and the number of grains was counted. Fig.7 shows the FGH95 bulk material metallographic image and the grain boundaries that have been outlined within the area of $227\ \mu\text{m} \times 174\ \mu\text{m}$. It can be seen from Fig.7 that the grains of FGH95 alloy are coarse and there exist several primary particle boundaries (PPB) before machining. Statistical analysis for grains size and numbers in Fig.7 of metallographic image is shown in Fig.8.

According to the grain equivalent diameter, the grains size of FGH95 can be divided into three grades: large grains, medium grains and small grains. When the grain equivalent diameter is less than $10\ \mu\text{m}$, it belongs to the small grains. When the grain equivalent diameter is between $10\ \mu\text{m}$ and $20\ \mu\text{m}$, it belongs to medium ones, and the large grain equivalent diameter is more than $20\ \mu\text{m}$. It can be drawn from Fig.8 that small grains amount to 31.03%, medium grains amount to 51.73%, and large grains amount to 17.24% of all the grains before the FGH95 is machined (that is for the bulk material of FGH95).

The same methods can be used to investigate the grain sizes in the machined surface generated under different cutting speeds. Fig.9 shows the FGH95 machined surface metallographic images in the area of $227\ \mu\text{m} \times 174\ \mu\text{m}$, which were obtained at various cutting speeds. The influence of cutting speed on grain numbers at the same area of $227\ \mu\text{m} \times 174\ \mu\text{m}$ is shown in Fig.10.

It can be seen from Fig. 10 that grain numbers within the sampling area increase with the increasing of cutting speed. This is a reflection of grains refinement. The higher cutting speeds can induce to the more serious grains refinement.

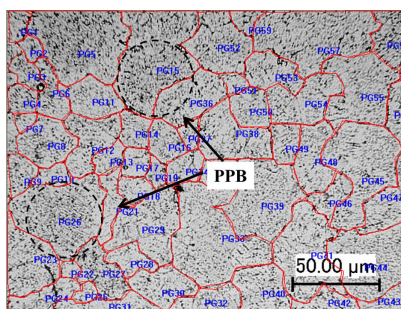


Fig.7 FGH95 bulk material metallographic image

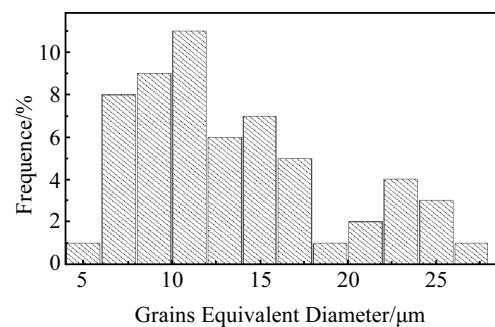


Fig.8 Statistics analysis for FGH95 bulk grains equivalent diameter

Statistical analysis for grains size and numbers obtained at various cutting speeds is shown in Fig.11.

In Fig.11, it can be drawn that cutting speed has significant effect on FGH95 alloy grains sizes. With the increasing of cutting speed, the number of large grains and medium grains continue to decrease while the small grain numbers increase for FGH95 alloy machined surface. This indicates that dynamic recrystallization occurs in the large grains and medium grains during the cutting process, which leads to the generation of dislocations during the cutting process of FGH95 alloy. The dislocations generated during cutting process are too late to cancel, owing to the material rapid deformation rate. When the cutting process continues, the number of dislocations increases, nucleation of grains recrystallization increases, which refines the grains. With the increasing of cutting speed, more dislocations are generated. More time to cancel the dislocation leads to the increasing of grains recrystallization nucleation, and thus severe grains refinement will occur. In addition, the original large grains are broken by shear and compression loads in cutting process, and small grains are then increased.

2.3 White layer microhardness

The microhardness of the white layer on the machined surface is higher than that of the bulk material due to work hardening property of FGH95 superalloy. Microhardness of white layer was measured in this study. The measurements were taken three times and the average result for each machined surface was recorded. The results of microhardness versus the cutting speeds are shown in Fig.12.

It can be seen from Fig.12 that the higher the cutting speeds, the higher the microhardness of the white layer. The higher hardness generated is mainly due to the cutting plastic deformation which is induced by corner radius extrusion and the severe friction between the tool flank face and machined surface. Surface materials endure significant strain hardening induced by surface deformation during the cutting process.

2.4 White layer residual stress

Residual stress is a type of inherent stress that maintains stress balance in the inner material when the components are unaffected by external strength^[33]. Residual stress generated

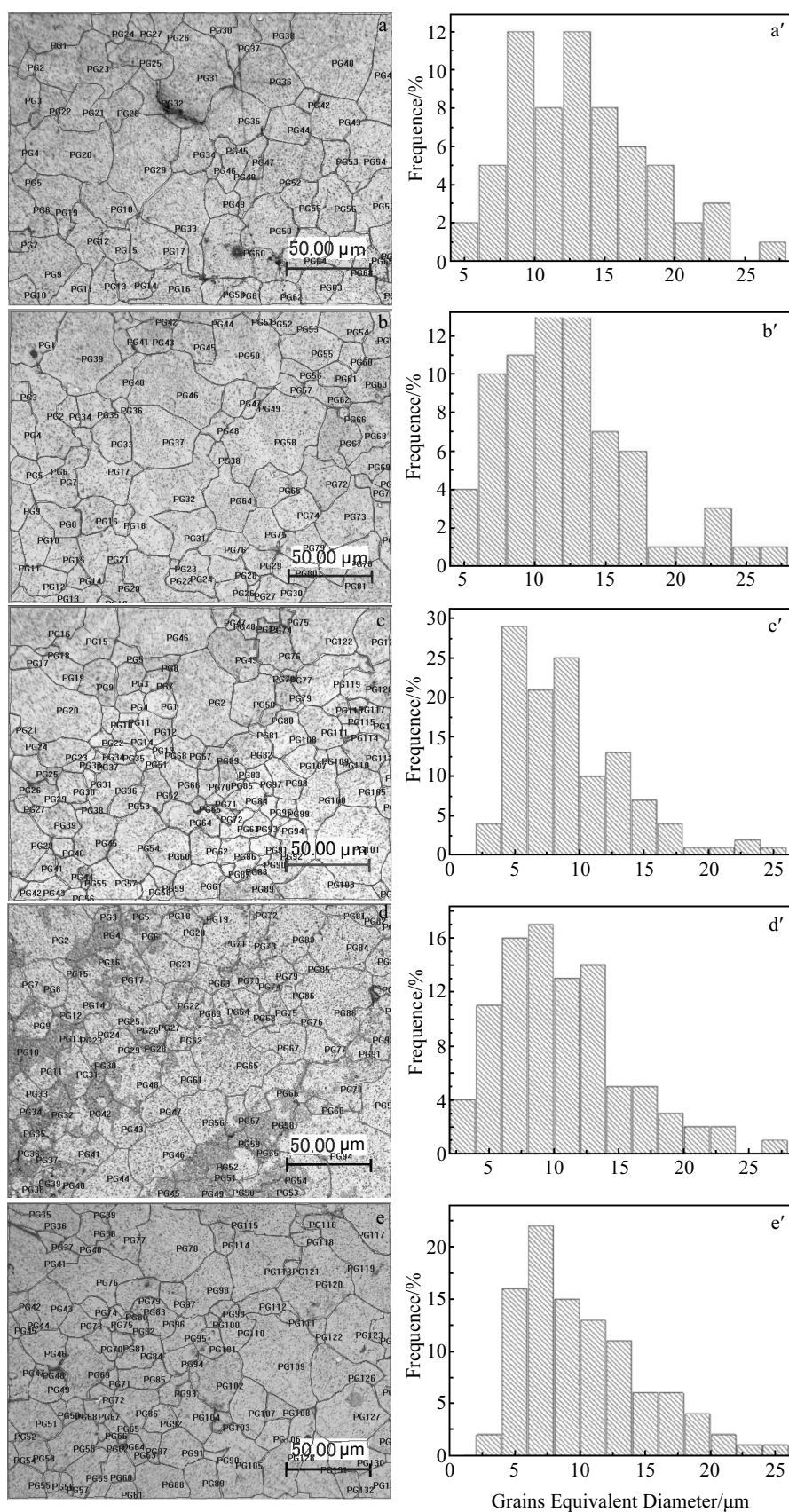


Fig.9 Machined surface metallographic images (a~e) and grains size statistical analysis (a'~e') at different cutting speeds: (a, a') $v=40$ m/min, (b, b') $v=80$ m/min, (c, c') $v=120$ m/min, (d, d') $v=160$ m/min, and (e, e') $v=200$ m/min

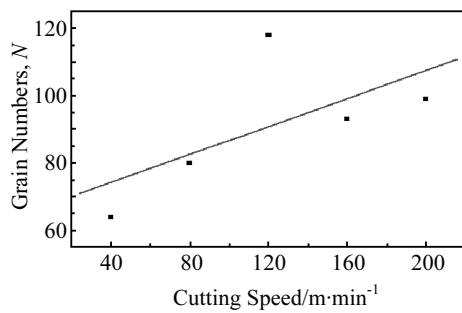


Fig. 10 Influence of cutting speed on grains numbers

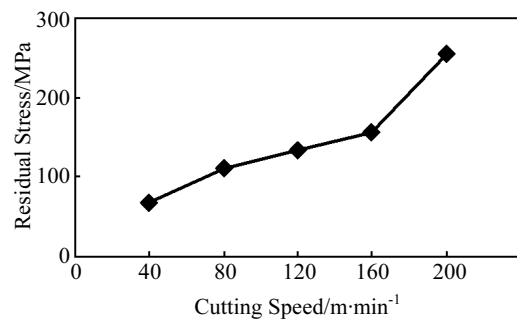


Fig. 13 Variation of surface residual stress with cutting speed

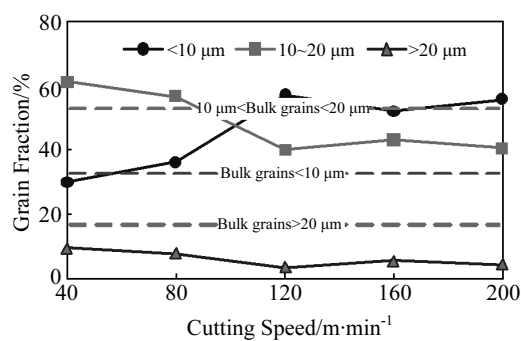


Fig. 11 Statistical analysis FGH95 machined surface grains size

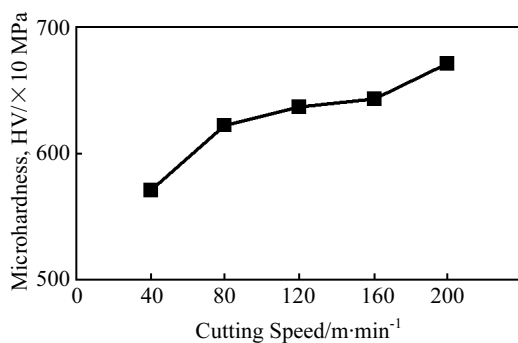


Fig. 12 Variation of machined surface microhardness with cutting speed

in the machined surface is usually harmful, which can reduce the resistance to fatigue strength, brittleness fracture, stability of the size and shape of the components. The residual stress in FGH95 machined surface was measured by the X-ray stress analyzer-Xstress 3000. The measurement results of machined surface residual stress obtained at various cutting speed is shown in Fig.13. It can be seen from Fig.13, residual stresses of FGH95 machined surface generated at various cutting speeds are all positive ones, and it means that residual stresses at FGH95 machined surfaces are residual tensile stresses. The residual tensile stresses have an increasing trend when cutting speed increases. That is the residual stress of white layer

increases with the white layer thickness increasing. This conclusion is the same as Kato's measurement results [34]. It can be drawn that the fatigue life of FGH95 machined surface decreases with the increasing of cutting speed.

3 Conclusions

1) White layer exhibits significantly different microstructures from the bulk materials. It shows densification, with no obvious structural features characteristic. With the increasing of cutting speed, the white layer thickness increases. White layer thickness is about 2.5~6.2 μm on the machined surface of FGH95 superalloy.

2) FGH95 superalloy bulk material exists in the form of Ni-based solid solution. The microstructure and the phase of Ni-based solid solution transform during the cutting process.

3) The high cutting speed induces serious grains refinement. With the increasing of cutting speed, the number of large grains and medium grains continue to decrease while the small grain numbers increase for machined surface of FGH95 superalloy.

4) The higher the cutting speeds, the higher the microhardness of the white layer.

5) Residual stresses of machined surface for FGH95 superalloy generated at various cutting speeds are all residual tensile stresses. As the cutting speed increases, the residual tensile stresses have an increasing trend.

References

- 1 Darwish S M. *International Journal of Adhesion & Adhesives*[J], 2000, 20: 279
- 2 Salak A, Vasiko K, Selecka M et al. *Journal of Materials Processing Technology*[J], 2006, 76: 62
- 3 Etienne R P, Carl B, Pelletier S et al. *Journal of Metallurgical and Materials Transactions*[J], 2007, 38: 1330
- 4 Choudhury I A, El-Baradie M A. *Journal of Materials Processing Technology*[J], 1998, 77: 278
- 5 Xu Kaitao, Zou Bin, Huang Chuanzhen et al. *Chinese Journal of Mechanical Engineering*[J], 2015, 28(3): 599
- 6 Bosheh S S, Mativenga P T. *International Journal of Machine Tools & Manufacture*[J], 2006, 46: 225

- 7 Herbert C R J, Axinte D A, Hardy M C et al. *Procedia Engineering*[J], 2011, 19: 138
- 8 Bushlya V, Zhou J M, Lenrick F et al. *Procedia Engineering*[J], 2011, 19: 60
- 9 Xu L Q, Clough S, Howard P et al. *Journal of Wear*[J], 1995, 181-183: 112
- 10 Attanasio A, Umbrello D, Cappellini C et al. *Journal of Wear*[J], 2012, 286-287: 98
- 11 Yang Y Y, Fang H S, Huang W G. *International Journal of Tribology*[J], 1996, 29: 425
- 12 Zhou Shaoping, Shen Yehui, Zhang Hao et al. *Chinese Journal of Mechanical Engineering*[J], 2015, 28(1): 140
- 13 Ranganath S, Guo C, Hegde P. *CIRP Annals-Manufacturing Technology*[J], 2009, 58: 77
- 14 Aramcharoen A, Mativenga P T. *International Journal of Advanced Manufacturing Technology*[J], 2008, 36: 650
- 15 Guo Y B, Schwach D W. *Materials Science and Engineering*[J], 2005, 395(A): 116
- 16 Akcan S, Shan S, Moylan S P et al. *Journal of Metallurgical and Materials Transactions A-physical Metallurgy and Materials Science*[J], 2002, 33: 1245
- 17 Thakur A, Gangopadhyay S. *International Journal of Machine Tools & Manufacture*[J], 2016, 100: 25
- 18 Jin D, Liu Z Q. *International Journal of Advanced Manufacturing Technology*[J], 2013, 68: 1573
- 19 Jin D, Liu Z Q. *Applied Surface Science*[J], 2014, 292: 197
- 20 Klocke F, Vogtel P, Gierlings S et al. *Production Engineering*[J], 2013(7): 593
- 21 Hosseini S B, Klement U, Yao Y et al. *Acta Materialia*[J], 2015, 89: 258
- 22 Hosseini S B, Beno T, Johansson S et al. *Journal of Materials Processing Technology*[J], 2014, 214(6): 1293
- 23 Hosseini S B, Dahlgren R, Klement U et al. *Procedia CIRP*[J], 2014, 14: 107
- 24 Veldhuis S C, Dosbaeva G K, Elfizy A et al. *Journal of Materials Engineering and Performance*[J], 2010, 19: 1031
- 25 Knight W A, Boothroyd G. *Fundamentals of Metal Machining and Machine Tools*[M]. Boca Raton: CRC Press, 2006: 195
- 26 Guo Y B, Warren A W, Hashimoto R. *CIRP Journal of Manufacturing Science and Technology*[J], 2010(2): 129
- 27 Guo Y B, Schwach D W. *International Journal of Fatigue*[J], 2005, 27: 1051
- 28 Siva P D, Shola A C, Srinivasa P B. *Materials Science & Engineering A*[J], 2014, 591: 78
- 29 Cheng Zhengkun, Liao Ridong. *Chinese Journal of Mechanical Engineering*[J], 2015, 28(6): 1141
- 30 Zhang S H, Hu B F, Li H Y et al. *Journal of University of Science and Technology Beijing*[J], 1993(1): 1
- 31 Xu Y H, Fang L, Cen Q H et al. *Journal of Wear*[J], 2005, 258: 537
- 32 Sangil H, Shreyes N M, Haluska M S et al. *Journal of Materials Science and Engineering A*[J], 2008, 488: 195
- 33 Song Wentao, Xu Chuanguang, Pan Qinxue et al. *Chinese Journal of Mechanical Engineering*[J], 2016, 29(2): 365
- 34 Kato T, Sugeta A, Nakayama E. *Journal of Wear*[J], 2011, 271: 400

粉末高温合金加工表面显微结构和力学性能变化研究

杜 劲, 张静婕, 王立国

(齐鲁工业大学, 山东 济南 250353)

摘 要: 在切削加工粉末高温合金过程中, 严重的塑性变形导致已加工表面出现显微组织结构和力学性能的变化。在已加工表面出现的白层体现出加工表面显微结构和力学性能的变化, 对高温合金加工表面质量的影响至关重要。为了揭示粉末高温合金已加工表面显微组织结构和力学性能的变化, 开展了切削速度对粉末高温合金 FGH95 已加工表面白层形成影响的研究。研究发现随着切削速度的提高, FGH95 高温合金已加工表面出现的白层厚度增大。对加工表面进行显微观察发现在表面覆盖着一层致密的、无明显组织特征的白层结构。通过对加工前后材料的 XRD 测试分析得出 FGH95 粉末高温合金基体材料以 Ni 基固溶体的形式存在, 而加工之后表面的显微组织结构则明显与基体材料不同。这说明在切削过程中粉末高温合金已加工表面发生了 Ni 基固溶体组织结构的变化。对 FGH95 高温合金已加工表面进行晶粒度测量发现, 切削速度越高晶粒细化现象越明显。对高温合金切削表面白层进行力学性能测试表明, 白层的显微硬度随着切削速度的提高而增大; 存在于高温合金已加工表面白层中的残余应力为拉应力, 且随着切削速度的提高拉应力增大。粉末高温合金已加工表面显微结构和力学性能变化研究可以揭示高温合金表面完整性的形成机理, 为已加工表面质量的预测和控制提供理论依据。

关键词: 粉末高温合金; 加工表面; 相变; 硬度测试; 残余应力

作者简介: 杜 劲, 男, 1985 年生, 博士, 副教授, 齐鲁工业大学机械与汽车工程学院, 山东 济南 250353, E-mail: dj84105@126.com